Yi Chen[1]
Lecturer
Mem. ASME
e-mail: leo.chen.yi@live.co.uk

Zhong-Lai Wang
Associate Professor
Mem. ASME
e-mail: wzhonglai@uestc.edu.cn

Jing Qiu
Lecturer
Mem. ASME
e-mail: qiujing@uestc.edu.cn

Hong-Zhong Huang
Professor
Mem. ASME
e-mail: hzhuang@uestc.edu.cn

School of Mechatronics Engineering,
University of Electronic Science and Technology
of China,
Chengdu 611731, China

Hybrid Fuzzy Skyhook Surface Control Using Multi-Objective Microgenetic Algorithm for Semi-Active Vehicle Suspension System Ride Comfort Stability Analysis

A polynomial function supervising fuzzy sliding mode control (PSFαSMC), which embedded with skyhook surface method, is proposed for the ride comfort of a vehicle semi-active suspension. The multi-objective microgenetic algorithm (MOμGA) has been utilized to determine the PSFαSMC controller's parameter alignment in a training process with three ride comfort objectives for the vehicle semi-active suspension, which is called the "offline" step. Then, the optimized parameters are applied to the real-time control process by the polynomial function supervising controller, which is named "online" step. A two-degree-of-freedom dynamic model of the vehicle semi-active suspension systems with the stability analysis is given for passenger's ride comfort enhancement studies, and a simulation with the given initial conditions has been devised in MATLAB. *The numerical results have shown that this hybrid control method is able to provide real-time enhanced level of reliable ride comfort performance for the semi-active suspension system.*
[DOI: 10.1115/1.4006220]

1 Introduction

The ride comfort is one of the most important characteristics for a vehicle suspension system, which is concerned with the feeling of the passengers in the running conditions and mainly arises from the various sources of vibrations of the vehicle body. Usually, a major source exciting of the vibration comes from the road surface irregularities which range from the standard test roads to the random variations of the road surface elevation profile through the vehicle suspension system.

As shown in Fig. 1, the main components of a vehicle suspension system include vehicle body, springs, dampers, and tires, in which (I) is a passive suspension system, in which the spring stiffness and damping coefficient values are fixed and cannot be adjusted in the suspension system's working process; (II) is a semi-active (SA) suspension system, which can only change the damping coefficient and does not invoke any energy inputs to the vehicle suspension system; and (III) is an active suspension system, which uses the actuator to exert an independent force on the suspension system to improve the ride characteristics and the needs for extra energy inputs.

The active suspension system has been investigated since the 1930s, but for the bottleneck of complexity and high cost of its hardware, it has been hard for a wide practical usage and it is only available on sports vehicles, military vehicles, or premium luxury vehicles [1]. The active suspension is designed to use the independent actuators to improve the suspension system's ride comfort performance. By reducing the vibration transmission and keeping proper tire contacts, the active and semi-active suspension systems are designed and developed to achieve better ride comfort performance than that of the passive suspension system. The SA suspension system was introduced in the early 1970s [2], it has been considered as a good alternative between the active and the passive suspension systems. The conceptual idea of SA suspension is to replace active force actuators with continually adjustable elements, which can vary or shift the rate of the energy dissipation in response to instantaneous condition of motion. The SA suspension system can only change the damping coefficient of the shock absorber, it will not add additional energy to the suspension system. The SA suspension system is also less expensive and energy consumptive than that of the active suspension system in operation [3]. In recent years, research on the SA suspension system has continued to advance with respect to their capabilities, narrowing the gap between the SA and the active suspension systems. The SA suspension system can achieve the majority of the performance characteristics of the active suspension system, which provides a wide class of practical applications. The magnetorheological/electrorheological (MR/ER) [4–7] dampers are both of the most widely studied and tested components of the SA suspension system. MR/ER fluids are materials that respond to an applied magnetic/electrical field with a change in rheological behavior. A dynamical model for the SA suspension system will be discussed as the control plant, in which the damping coefficient is adjustable.

The variable structure control (VSC) with sliding mode was introduced in the early 1950s by Emelyanov and was published in the 1960s [8], and further work was developed by several researchers [9–12]. The SA suspension system is one of the widely used VSC systems for the structural parameters keep changing in a motion process. Sliding mode control (SMC) has been recognized as a robust and efficient control method for the complex high order nonlinear dynamical systems and has also been applied to the MR/ER damper control for the SA suspension systems. The major advantage of sliding mode control is the low sensitivity to the changes of a system's parameters under various uncertainty conditions, and it can decouple system motion into independent partial components of lower dimension, which reduces the complexity of the system control and feedback design. The major drawback of traditional SMC is chattering, which is the

[1]Corresponding author.

Contributed by the Dynamic Systems Division of ASME for publication in the JOURNAL OF DYNAMIC SYSTEMS, MEASUREMENT, AND CONTROL. Manuscript received April 15, 2010; final manuscript received February 12, 2012; published online April 30, 2012. Assoc. Editor: Marcelo J. Dapino.

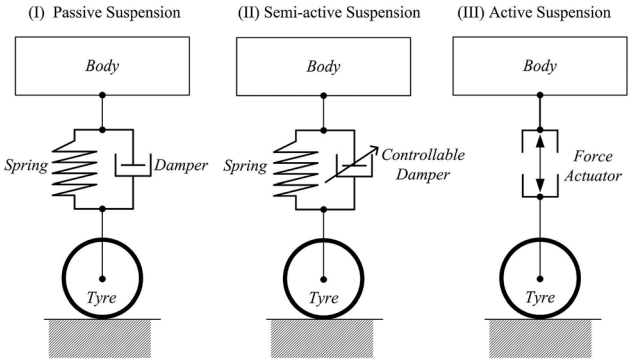

Fig. 1 Passive, semi-active, and active suspension systems

high frequency oscillation of the system outputs irritated by the discontinuous control switchings across sliding surface.

In order to deal with the chattering phenomenon, one of the widest known methods is the fuzzy logic theory. The fuzzy logic theory was first proposed by Zadeh [13] and was based on the concept of fuzzy sets. Fuzzy logic control (FLC) has been used in a wide variety of applications in engineering, such as in aircraft/spacecraft, automated highway systems, autonomous vehicles, washing machines, process control, robotics control, decision-support systems, portfolio selection, etc. Practically speaking, it is not always possible to obtain a precise mathematical model for nonlinear, complex or ill-defined systems. FLC is a practical alternative for a variety of challenging control applications, since it can provide a convenient method for constructing nonlinear controllers via the use of heuristic information (or knowledge). The heuristic information may come from an operator that acts as a "human-in-the-loop" controller and from whom experimental data are obtained. In recent years, a lot of literature has been generated in the area of fuzzy sliding mode control (FSMC) [11,14–28], which covered the chattering phenomenon of the traditional SMC design. The involvement of FLC in the design of the FSMC based controller can be harnessed to help reduce the chattering problem. The smooth control feature of fuzzy logic can be helpful in overcoming the disadvantages of chattering and this is why it can be useful to combine the FLC method with the SMC method, and thus to create the FSMC method. The involvement of FLC in the design of the FSMC based controller can be harnessed so as to help avoid the chattering problem. A fuzzy slide mode control with skyhook surface scheme will be discussed, and then based on which an improved control method supervised by a polynomial function will be proposed.

The skyhook control strategy was introduced by Karnopp et al. [2], it has been applied to reduce vertical vibration of the SA suspension system for its mathematical simplicity. The basic idea is to link the vehicle body sprung mass to the stationary sky by a controllable "skyhook" damper, which could reduce the vertical vibrations by the road disturbance of all kinds. Practically, there is no such stationary sky can be found as the mathematical assumption and the engineering product, but this point can be borrowed to design the sliding surface of a SMC with the assistance of FLC, this is one of the motivations for the new control method we will discuss in the sections below. The controller's parameter selection and optimization is another problem we need to solve with the objectives of passenger ride comfort, suspension deformation, and tire loads, the optimizer we will use in this context is genetic algorithms (GA).

The GA was introduced in the 1970s by John Holland [29] at University of Michigan. It is inspired by Darwin's theory about evolution by applying genetic operators, namely, selection, crossover, and mutation, to a population of individuals. Solution to a problem solved by GA is evolved; it has been widely studied, experimented, and applied in many fields in engineering. Many of the real world problems involved finding optimal parameters, which might prove difficult for traditional methods but ideal for GA [30–35]. The term micro-GA refers to a small population genetic algorithm with reinitialization, which was first introduced by Krishnakumar [36]. The idea of micro-GA was supported by some theoretical results obtained by Goldberg [37], according to which a population size of 3 was sufficient to converge, regardless of the chromosomal length. In this paper, the micro-GA method will be utilized as the optimizer for the parameters of the newly proposed polynomial function supervising fuzzy sliding mode controller, which will be then applied to the ride comfort control for a semi-active suspension system.

2 Two-Degree-of-Freedom Semi-Active Suspension System

The role of the vehicle suspension system is to support and isolate the vehicle body and payload from road disturbances, and maintain the traction force between tires and road surface. The SA suspension system can offer both the reliability and the versatility, such as passenger's ride comfort with less power demand. To achieve a basic understanding of the passenger's response to the vehicle's vibrational behavior, as given in Fig. 2, a two-degree-of-freedom (2-DOF) vehicle ride model which focuses on the passenger ride comfort performance is represented for an SA suspension system, in which m_1 and m_2 are the unsprung mass and the sprung mass, respectively; k_1 is the tire stiffness coefficient; k_2 and c_2 are the suspension stiffness coefficient and the suspension damping coefficient, respectively; c_e is the semi-active suspension damping coefficient, which can generate the semi-active damping force f_d by MR/ER absorber, as given in Eq. (2); z_1, z_2, and q are the displacements of the unsprung mass, the sprung mass, and the road disturbance, respectively; v_0 is the vehicle speed, which is the one of the input parameters for the road disturbance q; and g is the acceleration of gravity

$$\begin{cases} m_1\ddot{z}_1 + k_2(z_2 - z_1) + (c_2 + c_e)(\dot{z}_2 - \dot{z}_1) - k_1(z_1 - q) + m_1 g = 0 \\ m_2\ddot{z}_2 - k_2(z_2 - z_1) - (c_2 + c_e)(\dot{z}_2 - \dot{z}_1) + m_2 g = 0 \end{cases} \tag{1}$$

$$f_d = c_e(\dot{z}_2 - \dot{z}_1) \tag{2}$$

Using Newton's second law, the 2-DOF SA suspension model can be stated by Eq. (1), where f_d is the damping force as stated by Eq. (2)

$$\begin{cases} \dot{X} = AX + BQ + EU \\ Y = CX + DQ + FU \end{cases} \tag{3}$$

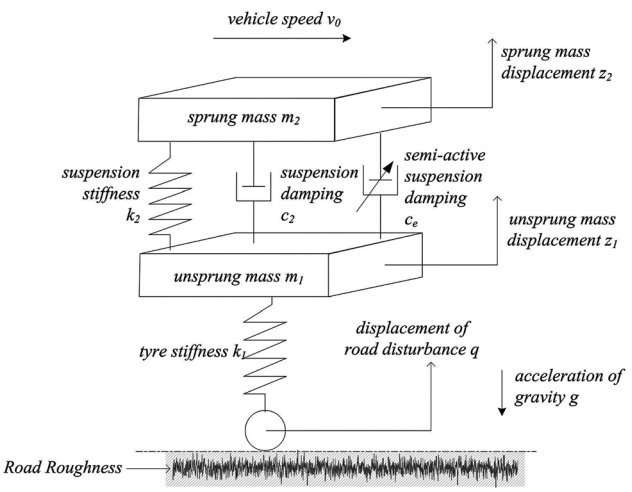

Fig. 2 Two-degree-of-freedom semi-active suspension system

$$X = \begin{Bmatrix} x_1 \\ x_2 \\ x_3 \\ x_4 \end{Bmatrix} = \begin{Bmatrix} z_1 - q \\ z_2 - z_1 \\ \dot{z}_1 \\ \dot{z}_2 \end{Bmatrix} \tag{4}$$

$$Y = \begin{Bmatrix} y_1 \\ y_2 \\ y_3 \end{Bmatrix} = \begin{Bmatrix} \ddot{z}_2 \\ z_1 - q \\ z_2 - z_1 \end{Bmatrix} \tag{5}$$

$$U = \{f_d\} \tag{6}$$

$$f_{\text{tire}} = k_1(z_1 - q) \tag{7}$$

$$Q = \begin{Bmatrix} \dot{q} \\ g \\ 0 \end{Bmatrix} \tag{8}$$

$$A = \begin{bmatrix} 0 & 0 & 1 & 0 \\ 0 & 0 & -1 & 1 \\ \dfrac{k_1}{m_1} & -\dfrac{k_2}{m_1} & \dfrac{c_2}{m_1} & -\dfrac{c_2}{m_1} \\ 0 & \dfrac{k_2}{m_2} & -\dfrac{c_2}{m_2} & \dfrac{c_2}{m_2} \end{bmatrix} \tag{9}$$

$$B = \begin{bmatrix} -1 & 0 & 0 \\ 0 & 0 & 0 \\ 0 & -1 & -\dfrac{1}{m_1} \\ 0 & -1 & \dfrac{1}{m_2} \end{bmatrix} \tag{10}$$

$$C = \begin{bmatrix} 0 & \dfrac{k_2}{m_2} & -\dfrac{c_0}{m_2} & \dfrac{c_0}{m_2} \\ 1 & 0 & 0 & 0 \\ 0 & 1 & 0 & 0 \end{bmatrix} \tag{11}$$

$$D = \begin{bmatrix} 0 & -1 & \dfrac{1}{m_2} \\ 0 & 0 & 0 \\ 0 & 0 & 0 \end{bmatrix} \tag{12}$$

$$E = \begin{Bmatrix} 0 \\ 0 \\ -\dfrac{1}{m_1} \\ \dfrac{1}{m_2} \end{Bmatrix} \tag{13}$$

$$F = \begin{Bmatrix} \dfrac{1}{m_2} \\ 0 \\ 0 \end{Bmatrix} \tag{14}$$

In order to observe the status of the 2-DOF SA suspension system, the Newton's second law equations, as given by Eq. (1), can be rewritten as the state-space equations in Eq. (3). The state-space analysis concerns three types of variables (input variables, output variables, and state variables) [11,38], as shown in Eqs. (4)–(6) [39] in the form of vectors (state vectors), in which X is the state vector for 2-DOF SA suspension system, which includes the tire deformation $(x_1 = z_1 - q)$, the suspension deformation $(x_2 = z_2 - z_1)$, the unsprung mass velocity $(x_3 = \dot{z}_1)$, and the sprung mass velocity $(x_4 = \dot{z}_2)$, as given in Eq. (4); Y is the output vector with three state variables for the 2-DOF SA suspension system, which includes the vehicle body acceleration $(y_1 = \ddot{z}_2)$, the tire deformation $(y_2 = z_1 - q)$, and the suspension deformation $(y_3 = z_2 - z_1)$, as given in Eq. (5); U is the input vector (control force vector) in Eq. (6); according to the tire deformation (y_2), the tire load can be stated in Eq. (7); Q is the external road disturbance vector in Eq. (8), which contains two external disturbance signals of road velocity profile and acceleration of gravity; and A, B, C, D, E, and F are the coefficient matrices in Eqs. (9)–(14).

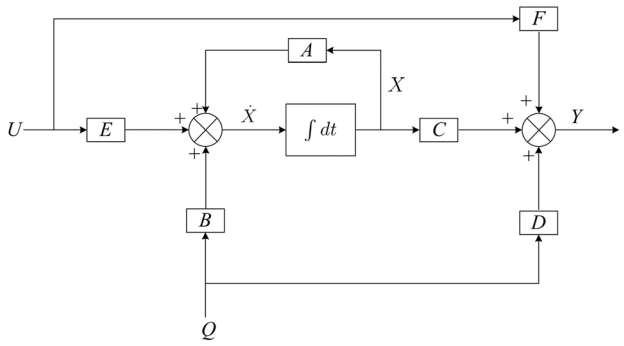

Fig. 3 Block diagram for the two-degree-of-freedom semi-active suspension system

In this context, it is convenient to select the measurable quantities as the state variables by a block diagram because the full-state feedback control law requires the feedback of all selected state variables with suitable weighting. The block diagram for the state-space equations is given in Fig. 3, which represents the 2-DOF SA suspension system for further controller design.

3 Sliding Mode Control With Skyhook Surface Scheme

As shown in Fig. 4, the skyhook control method is known as one of the most effective in terms of the simplicity of the control algorithm. The skyhook control can reduce the resonant peak of the sprung mass quite significantly and thus achieves a good ride quality by adjusting the skyhook damping coefficient when vehicle body velocity and other conditions are changing.

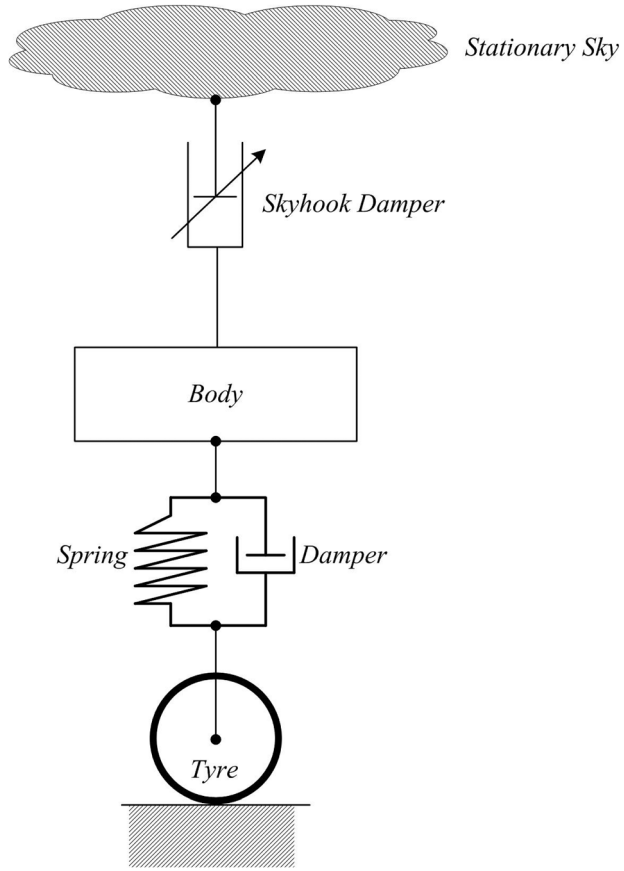

Fig. 4 Ideal skyhook damper definition, adopted from Karnopp et al. [2]

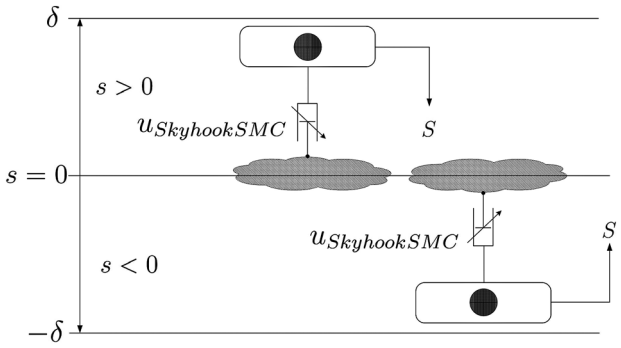

Fig. 5 Sliding mode surface with skyhook scheme [39–43]

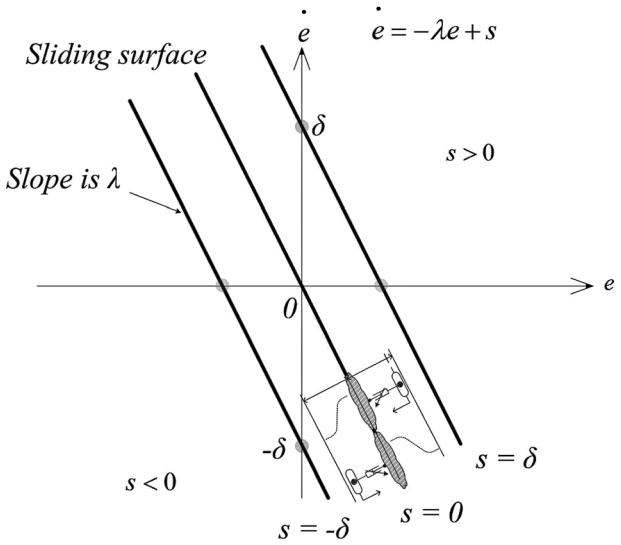

Fig. 6 Sliding surface generation with skyhook scheme [11,40–44]

By deriving this idea to reduce the sliding chattering phenomenon, a soft switching control law is introduced [39–43] for the major sliding surface switching activity in Eq. (19), as shown in Fig. 5, which is to reduce the chattering and achieve good switch quality for a sliding mode control with skyhook surface scheme (SkyhookSMC).

As shown in Fig. 6, when designing a SkyhookSMC, the objective is to consider the 2-DOF suspension system as the control plant, which is defined by the state-space equations, as stated in Eq. (3). s is the sliding surface of the hyperplane, which is given in Eq. (15), where λ is a positive constant that defines the slope of the sliding surface. As the 2-DOF SA suspension system is a second-order system, then it can be given $n=2$, in which s defines the position and velocity errors, and Eq. (15) can be rewritten as Eq. (16)

$$s(e,t) = \left(\frac{d}{dt} + \lambda\right)^{n-1} e \tag{15}$$

$$s = \dot{e} + \lambda e \tag{16}$$

$$V(s) = \frac{1}{2}s^2 \tag{17}$$

$$\dot{V}(s) = s\dot{s} \tag{18}$$

According to Eq. (16), the second-order tracking problem of 2-DOF SA suspension system is now being represented by a first-order stabilization problem, in which the scalar s is set to zero by means of a governing condition [11]. Obtained from the use of the Lyapunov stability theorem, the SkyhookSMC is designed that the origin is a globally asymptotically stable equilibrium point for the control system. The Lyapunov candidate function V and its time derivative function $\dot{V}$ are given in Eqs. (17) and (18), respectively. The energy-like Lyapunov candidate function V is positive definite. If the derivative function $\dot{V}$ satisfies the negative definite condition, the plant is in a stable status; if the derivative function $\dot{V}$ is positive definite, the plant performs unstably and meanwhile the controller needs to be activated, as defined in Eq. (19).

$$u_{\text{SkyhookSMC}} = \begin{cases} -c_0 \tanh\left(\frac{s}{\delta}\right) & s\dot{s} > 0 \\ 0 & s\dot{s} \le 0 \end{cases} \tag{19}$$

The smooth control time-function generated by the SkyhookSMC is expressed in Eq. (19), where c_0 is an assumed positive damping ratio for the switching control law. The SkyhookSMC law needs to be chosen in such a way that the existence and the reachability of the sliding mode are both guaranteed. It is noted that δ is an assumed positive constant, which defines the thickness of the sliding mode boundary layer [44].

4 Fuzzy Logic Control

Generally, in the FLC design methodology, the human operator needs to write down a set of rules about how to control the process, this is called the "rule-base," and then a fuzzy controller can emulate the decision-making process of the human by the rule-base, in which the heuristic information (knowledge) may come from a control engineer who has performed extensive mathematical modeling, analysis, and development of control algorithms for a particular process. Again, such expertise is loaded into the fuzzy controller to automate the reasoning processes and actions of the expert. Regardless of where the heuristic control knowledge comes from, fuzzy control provides a user-friendly formalism for representing and implementing the ideas which can help to achieve high-performance control [39–43,45,46].

As shown in Fig. 7, the fuzzy controller has four main components: A rule-base (a set of "IF-THEN" rules) contains a fuzzy logic quantification of the expert's linguistic description of how to achieve good control; an "inference mechanism," which emulates the expert's decision making in interpreting and applying knowledge about how efficiently to control the plant. A set of the IF-THEN rules are loaded into the rule-base, and an inference strategy is chosen, then the system is ready to be tested, and the closed-loop specifications are needed; a "fuzzification" interface, which converts "crisp" inputs into "fuzzy" information that the inference mechanism can be interpreted and compared to the rules in the rule-base; and a "defuzzification" interface, converts the conclusions by the inference mechanism into the FLC crisp (actual) outputs as the control inputs for the plant.

Briefly, fuzzy control system can be designed in the following steps: (1) choosing the fuzzy controller inputs and outputs, (2) choosing the preprocessing that is needed for the controller inputs and possibly postprocessing that is needed for the outputs, and (3) designing each of the four components of the fuzzy controller, as shown in Fig. 7, which includes fuzzification, inference mechanism, rule-base, and defuzzification.

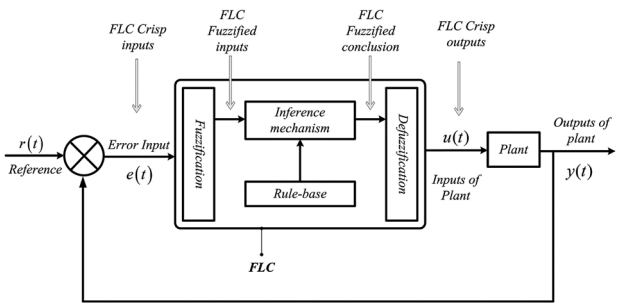

Fig. 7 Fuzzy logic controller architecture [43]

Table 1 Fuzzy linguistic values

Fuzzy linguistic value	Description	*E*	*EC*	*U*
NL	Negative large	−5	−5	−2
NM	Negative middle	−4	−4	−1.5
NS	Negative small	−3	−3	−1
ZE	Zero	0	0	0
PS	Positive small	3	3	1
PM	Positive middle	4	4	1.5
PL	Positive large	5	5	2

Fuzzification is the process of decomposing the system inputs into fuzzy sets. That is, it is to map variables from the crisp space to the fuzzy space. The process of fuzzification allows the system inputs and outputs to be expressed in linguistic terms so that rules can be applied in a simple manner to express a complex system. In the FLC for the 2-DOF SA suspension system, the velocity and acceleration of the vehicle body are selected as the crisp error (e) and the crisp change-in-error (ec) feedback signals for the 2-DOF SA suspension system control. There are seven linguistic terms in the fuzzy sets for two inputs of the fuzzified error (E) and the fuzzified change-in-error (EC), and one output of fuzzified force (U), which are *NL*, *NM*, *NS*, *ZE*, *PS*, *PM*, and *PL*, as stated in Table 1, and their linguistic values are also listed in it for further numerical simulation with proper ranges of [−5, 5] and [−2, 2]. Defuzzification is the opposite process of fuzzification, it is to map variables from fuzzy space to crisp space.

A membership function (MF) is a manner that defines how each point in the input space is mapped to a membership value between 0 and 1. The MF for the 2-DOF SA suspension system is a triangular-shaped membership function. The inputs of E and EC are interpreted from this fuzzy set, and the degree of membership is interpreted. The structure of the FLC for the 2-DOF SA suspension system is a standard 2-in-1-out FLC, and the IF-THEN rule-base is then applied to describe the experts' knowledge. The FLC rule-base is characterized by a set of linguistic description rules based on conceptual expertise, which arises from typical human situational experience. In particular, the 2-in-1-out FLC rule-base for the ride comfort of the 2-DOF SA suspension system is given in Table 2 [39], with two inputs and seven linguistic values for each of those, there are at most $7^2 = 49$ possible rules as following list:

(1) IF $E = NL$, AND $EC = NL$, THEN $U = PL$;
(2) IF $E = NL$, AND $EC = NM$, THEN $U = PL$;
(3) IF $E = NL$, AND $EC = NS$, THEN $U = PM$;
⋮
(49) IF $E = PL$, AND $EC = PL$, THEN $U = NL$.

Table 2 defines the relationship between two inputs of the fuzzified error (E) and the fuzzified change-in-error (EC) with one output of the fuzzified control force (U), which came from the previous experience gained for the semi-active damping force control during body acceleration changes for ride comfort. Briefly, the main linguistic control rules are (1) when the body acceleration and velocity increase, the SA damping force decrease; and (2) when the body acceleration and velocity decrease, the SA damping force increases.

Table 2 The 2-in-1-out FLC rule table for 2-DOF SA suspension system [39]

U		*EC*						
		NL	NM	NS	ZE	PS	PM	PL
E	NL	PL	PL	PM	PS	PS	PS	ZE
	NM	PL	PM	PS	PS	PS	ZE	NS
	NS	PM	PS	ZE	ZE	ZE	NS	NM
	ZE	PM	PS	ZE	ZE	ZE	NS	NM
	PS	PM	PS	ZE	ZE	ZE	NS	NM
	PM	PS	ZE	ZE	ZE	NS	NM	NL
	PL	ZE	NS	NS	NS	NM	NL	NL

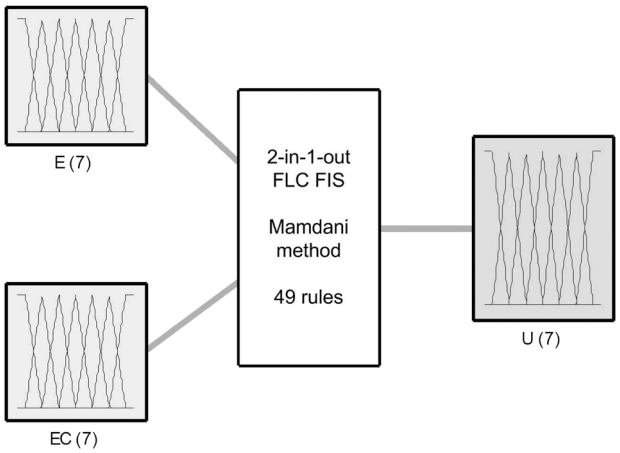

Fig. 8 The fuzzy inference system for 2-DOF SA suspension system

Fuzzy inference is the process of formulating the mapping from a given input to an output using fuzzy logic. The mapping then provides a basis from which decisions can be made, or patterns discerned. The process of fuzzy inference involves all of the pieces that are described in the previous sections: membership functions, logical operations, and IF-THEN rules. Mamdani's fuzzy inference method [47–49] is the most commonly seen fuzzy methodology, which was among the first control systems built using fuzzy set theory and was proposed in 1975 by Mamdani as an attempt to control a steam engine and boiler combination by synthesizing a set of linguistic control rules obtained from experienced human operators. Mamdani's effort was based on Zadeh's research [50] on fuzzy algorithms for complex systems and decision processes in 1973. The Fuzzy Inference System of Mamdani-type inference for the 2-in-1-out FLC is shown in Fig. 8.

5 Fuzzy Sliding Mode Control With Switching Factor α

A fuzzy sliding mode control with switching factor α (FαSMC) [40,41] was introduced to combine the FLC with the SkyhookSMC to deal with the chattering phenomenon, which has been harnessed to reduce the 2-DOF SA suspension system ride comfort control with proper parameter selection. A flow diagram for the FαSMC, applying the SkyhookSMC approach, is given in Fig. 9. The control effects of the FLC and the SkyhookSMC are combined by Eq. (20). In Eq. (20), α is a switching factor which balances the weight of the FLC to that of the SkyhookSMC.

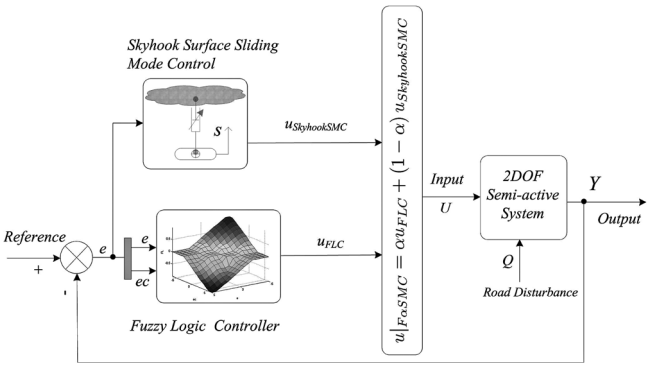

Fig. 9 FαSMC flow diagram

Clearly, $\alpha = 0$ represents SkyhookSMC, and $\alpha = 1$ represents FLC, $\alpha \in [0, 1]$, in which the SkyhookSMC has been discussed in Sec. 3 and the FLC has been discussed in Sec. 4

$$u_{F\alpha SMC} = \alpha u_{FLC} + (1 - \alpha) u_{SkyhookSMC} \tag{20}$$

6 Polynomial Function Supervising FαSMC—An Improvement

To make the necessary improvement to the FαSMC method, a hybrid real-time polynomial function [51] supervising FαSMC with skyhook surface (PSFαSMC) is proposed and then will be applied to the ride comfort control for the 2-DOF SA vehicle suspension system. The basic idea of PSFαSMC is to generate a series of supervising functions in polynomial function form which are optimized and produced by micro-GA in offline step [51], which is a training process for the PSFαSMC parameter selection. The supervising functions are to generate parameters for FαSMC in online real-time control step.

Briefly, there are two steps in PSFαSMC controller design: offline step and online step: (1) the offline step is to take the micro-GA as the optimizer to generate polynomial functions for each parameter in FαSMC, including K_e, K_{ec}, K_u, α, c_0, δ, and λ. In the micro-GA optimization process, each loop will take more time than practical real-time control required, and that is why the polynomial functions can be taken as practical real-time control parameter generators for online step; (2) the online step is to generate proper parameters by the polynomial functions, which came from offline step. In the online step, the polynomial functions are the real-time parameter generators, which supervise the FαSMC controller by adjusting its parameters.

The parameters' selection for FαSMC needs a lot of manual testing and time consuming. In order to reduce the working time in parameters' selection for this hybrid control method PSFαSMC, the micro-GA is to be applied as the optimizer to generate proper results for parameters selection, which has been widely applied into industrial applications [52–56].

6.1 Multi-Objective Micro-GA for the Offline Step. The population size in GA usually goes from tens to hundreds, sometimes to thousands. With such a number of individuals, it can lead to formidable calculation time consumption. It is important to design high efficient GA for multi-objective optimization problems. One of the popular methods in this direction is the micro-GA with a very small internal population (3→6 individuals) [52]. As shown in Fig. 10, generally, there are two loops in the MOμGA process: internal cycle and external cycle; meanwhile, there are also two groups of population memories: the internal population memory, which is used as the source of diversity of the micro-GA internal loop; and the external population memory, which is used to archive individuals of the Pareto optimal set. In the internal loop, the internal population memory is divided into two parts: a replaceable part and a nonreplaceable part, whose percentages of each part can be adjusted by the user. In the elitism block, the Pareto ranking methods are taken into process inside internal cycle, which could include Deb–Goldberg method [57], Goldberg's method [58], or Fonseca–Fleming method [59].

For the small internal population, mutation is an optional operator for micro-GA. Practically, there are three parts in micro-GA optimization: (1) fitness functions definition, (2) encoding and decoding definition, and (3) genetic operators definition, which includes selection, crossover, and mutation. Once the three parts have been well defined, the micro-GA can then create a population of solutions and apply genetic operators such as mutation and crossover to evolve the solutions in order to find better results.

As defined in Eq. (5), the output matrix Y contains three state variables for the 2-DOF SA suspension system, which are related to the ride comfort performance, including vehicle body acceleration (y_1), tire deformation (y_2), and suspension deformation (y_3).

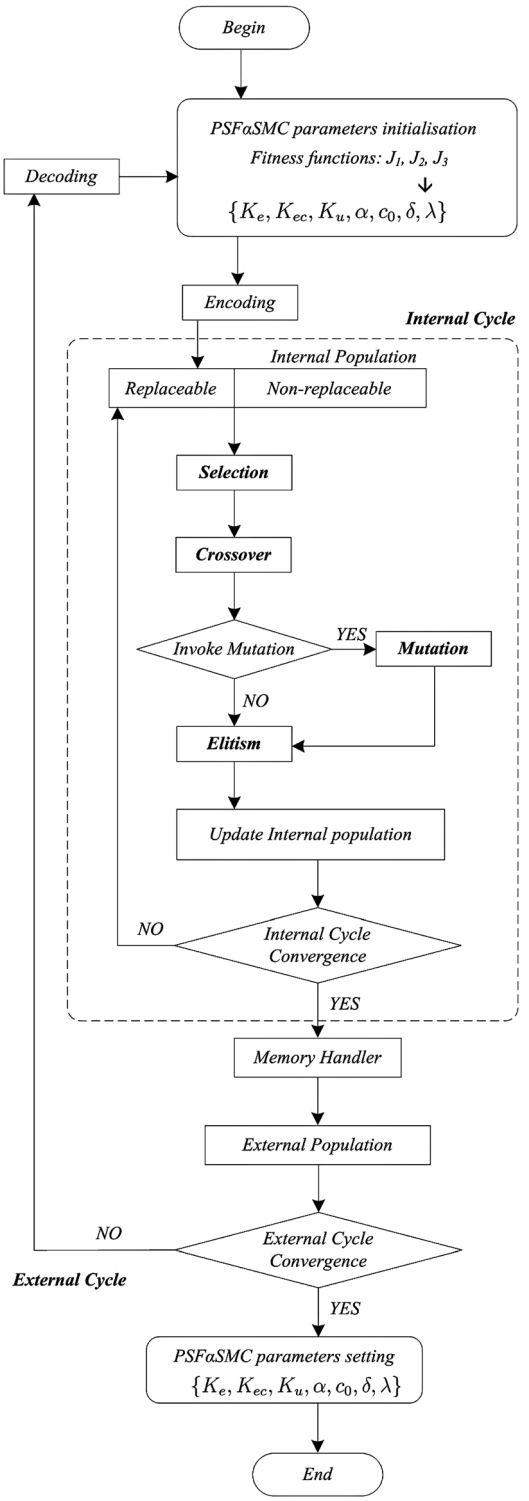

Fig. 10 Microgenetic algorithm for PSFαSMC work flow diagram

$H(Y)$ is the error state function, as defined in Eq. (21), which can generate the error state variables (e_1, e_2, and e_3) for three output state variables (y_1, y_2, and y_3). $y_1|_{ref}$, $y_2|_{ref}$, and $y_3|_{ref}$ are the reference state variables for the PSFαSMC

$$H(Y) == \begin{Bmatrix} e_1 \\ e_2 \\ e_3 \end{Bmatrix} = \begin{Bmatrix} y_1 - y_1|_{ref} \\ y_2 - y_2|_{ref} \\ y_3 - y_3|_{ref} \end{Bmatrix} = \begin{Bmatrix} \ddot{z}_2 - y_1|_{ref} \\ z_1 - q - y_2|_{ref} \\ z_2 - y_3|_{ref} \end{Bmatrix} \tag{21}$$

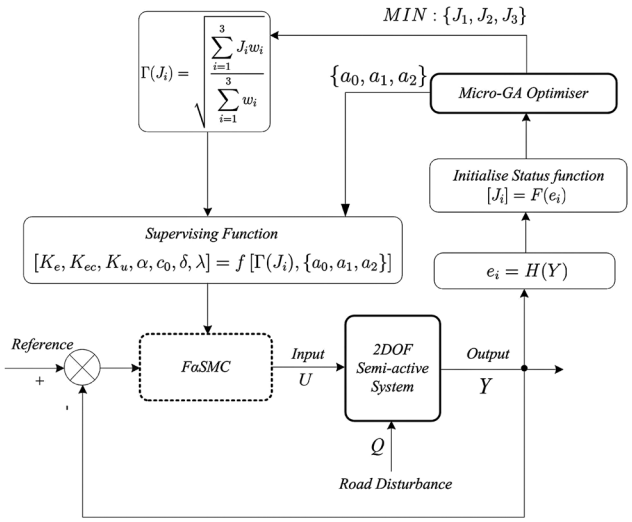

Fig. 11 PSFαSMC offline step—training

As shown in Fig. 11, in the PSFαSMC offline step, micro-GA is to optimize and generate polynomial functions for each parameter (K_e, K_{ec}, K_u, α, c_0, δ, and λ), and there are three fitness values for three objectives as J_i, as stated in Eq. (22), $F(*)$ is the function for the fitness function, RMS[*] is the function for the values of root mean square

$$J_i = F(e_i) = MIN\{RMS[ITAE(e_i)]\}, \quad i = 1, 2, 3 \tag{22}$$

According to International Standards Organization (ISO) 2631 [60], the ride comfort is specified in terms of RMS acceleration over a frequency range, then the fitness functions (J_i) for the 2-DOF SA suspension system are the functions of the error state variables (e_i), which are the values of root mean square (RMS[*]) of the integral of time times the absolute error (ITAE) performance indexes, that is, J_1, J_2, and J_3 are the RMS of ITAE indexes for the error state variables: body acceleration (e_1), suspension deformation (e_2), and tire loads (e_3), respectively. The ITAE of the error state variables (e_i) is expressed in Eq. (23)

$$ITAE(e_i) = \int_0^\infty t|e_i(t)|dt \tag{23}$$

As stated in Eq. (22), the micro-GA's optimizing criteria are to minimize the fitness functions (J_i) and to generate a set of solutions for the better supervising function parameters (K_e, K_{ec}, K_u, α, c_0, δ, and λ) via the interval arguments a_1, a_2, a_3, and Γ, which will be discussed in Sec. 6.2. Then, the micro-GA can provide the optimality of a set of solutions for the multi-objective applications of the ride comfort control in the online step, and the engineers can try each of the solution or select the solution by proper policy, e.g., outer range, inner range, or average of the Pareto set as an engineering solution. In the optimization process by micro-GA, binary encoding/decoding, roulette-wheel selection, and single point crossover are taken in micro-GA evolutional process. In the micro-GA optimization process, the initial conditions need to be given to the seven design variables, as given in Table 5.

6.2 Offline Step. As shown in Fig. 11, the offline step is a training process to optimize and generate a series of polynomial functions for further use in online step, and the micro-GA is the optimizer as discussed in Sec. 6.1

$$f[\Gamma(J_i), \{a_0, a_1, \ldots, a_N\}] = a_N\Gamma(J_i)^N + a_{N-1}\Gamma(J_i)^{N-1} + \cdots + a_2\Gamma(J_i)^2 + a_1\Gamma(J_i) + a_0 \tag{24}$$

As stated in Eq. (24), $f[\Gamma(J_i),\{a_0, a_1, \ldots, a_N\}]$ is the supervising function in polynomial form, which is fitted by the least square principle based on output data from the micro-GA optimization block, where N is a positive integer, a_0, a_1, …, a_N are constant coefficients

$$\Gamma(J_i) = \sqrt{\frac{\sum_{i=1}^{3} J_i w_i}{\sum_{i=1}^{3} w_i}} \tag{25}$$

$\Gamma(J_i)$ is a component of the polynomial supervising function $f[\Gamma(J_i),\{a_0, a_1, \ldots, a_N\}]$, as defined in Eq. (25), which is a weighted index by the optimized 2-DOF SA suspension ride comfort indexes J_i

$$f[\Gamma(J_i), \{a_0, a_1, a_2\}] = a_2J_i^2 + a_1J_i + a_0 \tag{26}$$

Basically, a smooth supervising function curve is required in the SA suspension system ride comfort control, $N = 2$ is chosen as the highest degree of the supervising polynomial functions. The polynomial function with $N = 2$ can provide the acceptable accurate outputs with the relatively low central processing unit (CPU) time consumptions, that is, the $N = 2$ polynomial function is with a relatively high accuracy versus time-consumption ratio in engineering applications [51]. Equation (26) is for the parameter K_e generation, and the similar processes will go with other parameters. There are seven supervising functions for the seven PSFαSMC parameters (K_e, K_{ec}, K_u, α, c_0, δ, and λ), as given in Eq. (27). As shown in Fig. 11, the supervising functions will be applied to the FαSMC block

$$\begin{cases} K_e = f[\Gamma(J_i), \{a_0, a_1, a_2\}]|_{K_e} \\ K_{ec} = f[\Gamma(J_i), \{a_0, a_1, a_2\}]|_{K_{ec}} \\ K_u = f[\Gamma(J_i), \{a_0, a_1, a_2\}]|_{K_u} \\ \alpha = f[\Gamma(J_i), \{a_0, a_1, a_2\}]|_{\alpha} \\ c_0 = f[\Gamma(J_i), \{a_0, a_1, a_2\}]|_{c_0} \\ \delta = f[\Gamma(J_i), \{a_0, a_1, a_2\}]|_{\delta} \\ \lambda = f[\Gamma(J_i), \{a_0, a_1, a_2\}]|_{\lambda} \end{cases} \tag{27}$$

6.3 Online Step. As shown in Fig. 12, the online step is to apply the polynomial functions to supervise the FαSMC for the 2-DOF SA suspension system. There are seven design variables (K_e, K_{ec}, K_u, c_0, δ, λ, and α) in PSFαSMC in the online step, which are given in Eq. (27). As stated in Eq. (27), the supervising functions are the functions of $\Gamma(J_i)$, a_0, a_1, and a_2, which can generate the parameters for the FαSMC over the real-time simulation. In Fig. 12, the polynomial functions are optimized data source for FαSMC parameters (K_e, K_{ec}, K_u, α, c_0, δ, and λ), which have been produced in offline step, which include that K_e is FLC scaling gains for e; K_{ec} is FLC scaling gains for ec; K_u is FLC scaling gains for u; c_0 is SkyhookSMC damping coefficient; δ is the thickness of the sliding mode boundary layer; λ is the slope of the sliding surface; and α is the switching factor of FαSMC in PSFαSMC.

7 Road Surface Profile—The Modeling of the Source of Uncertainty

To simulate the road excitation for the vehicle suspension system, a road profile is defined as the cross-sectional shape of a road surface under the given conditions, which can be expressed by statistical procedures [61,62]. There are a few types of excitations for the road surface profile, such as sine waves, step functions, and triangular waves, which can provide a basis for comparative studies under some simple road surfaces, but these can hardly serve as a valid and general basis for a practical road roughness of

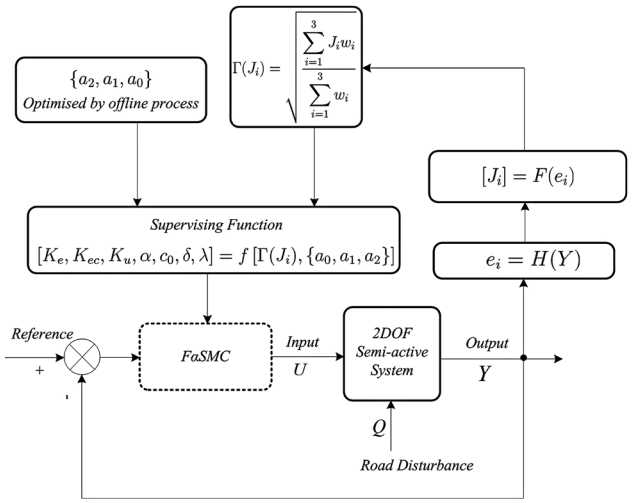

Fig. 12 PSFαSMC online step—control for SA suspension system

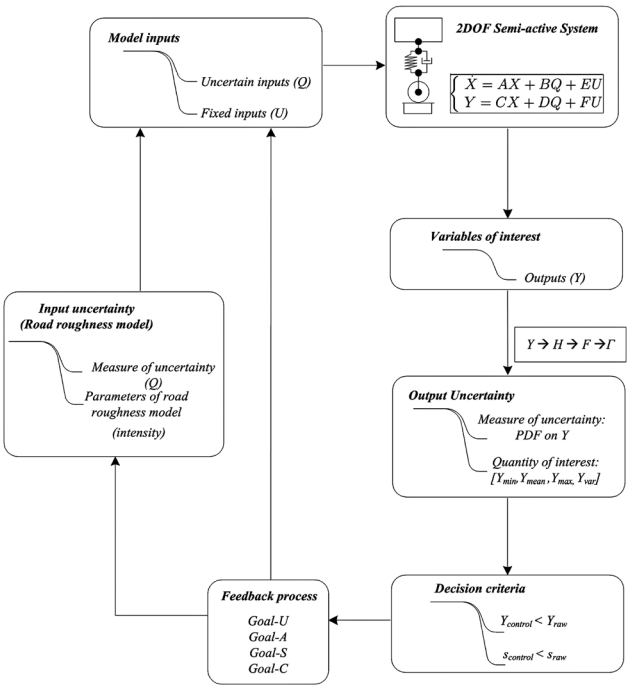

Fig. 13 Uncertainty analysis framework for vehicle suspension system ride comfort

ride behavior. As shown in Fig. 2, it is more realistic to describe a road surface profile as a random function or data sequence—the road roughness. There are some existing methods such as the International Roughness Index values and the Fourier transform-based sequence, described in the ISO 8608:1995 "Mechanical Vibration—Road Surface Profiles—Reporting of Measured Data" [63]; however, both only give an average condition for a relatively long section of the pavement.

A widely used statistical way to generate road excitation is to describe the road roughness using power spectral density (PSD). When the road surface profile is regarded as a random function, it can be characterized by a PSD function [64]. To classify the roughness (irregularities) of road surfaces, the International Standards Organization has proposed a road roughness classification, roughness-A (very good) to roughness-H (very poor) based on the PSD, in which the relationships between the PSD function $S_g(\Omega)$ and the spatial frequency Ω for different classes of road roughness can be approximated by two straight lines with different slopes on a log−log scale, which can be expressed as Eq. (28) [65], and the values of N_1 and N_2 are 2.0 and 1.5, respectively. In this case, to generate the road profile of a random base excitation for the 2-DOF SA suspension simulation, a spectrum of a geometrical road profile with road class "roughness-C" is considered, and Ω_0 is the reference spatial frequency. The vehicle is travelling at a constant speed v_0, and the historical road irregularity is given by the PSD method [66–68]

$$\begin{cases} S_g(\Omega) = S_g(\Omega_0)\left(\dfrac{\Omega}{\Omega_0}\right)^{-N_1}, & \Omega \le \Omega_0 = \dfrac{1}{2\pi}\, cycles/m \\ S_g(\Omega) = S_g(\Omega_0)\left(\dfrac{\Omega}{\Omega_0}\right)^{-N_2}, & \Omega > \Omega_0 = \dfrac{1}{2\pi}\, cycles/m \end{cases} \tag{28}$$

8 Uncertainty Studies

As shown in Fig. 13 [69], the uncertainty analysis with a feedback loop is proposed corresponding to the PSFαSMC online step control process as discussed in Sec. 6.3. The goal of the 2-DOF SA suspension system modeling is primarily the demonstration of compliance with uncertainty criteria embodied by the target values in the guidelines (Goal-U, -A, -S, and -C) as given in Table 3 [69]. According to Fig. 13 and Table 3, a metrological chain is compared to investigate which complies best with the proper criteria guidelines (Goal-A, -S, and -C). Through the establishment of industrial emission practices, it also appears that understanding the importance of the various sources of uncertainty will become even more important in improving the metrological options in the long term (Goal-U).

Primarily, two uncertainty variables of interest are considered as listed in Fig. 13: the 2-DOF SA suspension vehicle body acceleration Y and sliding surface s. Based on the International Standard in Metrological Uncertainty (GUM) [70], the target values specified by the uncertainty decision criteria: A quantity of interest representing the relative uncertainty is compared to a maximal percentage of relative uncertainty.

9 Uncertainty Propagation and Simulations

All the results for the ride comfort are obtained by using the parameters for the 2-DOF SA vehicle suspension system and

Table 3 The goals of the quantitative uncertainty assessment [69]

Type	Goal
Goal-U(understand)	To understand the importance of uncertain, then to establish the measurement and modeling.
Goal-A(accredit)	To give credit to a method of measurement, and to reach an acceptable quality level for its use. This may involve calibrating sensors, estimating the parameters of the model inputs.
Goal-S(select)	To compare relative performance and optimize the choice of objective policy, operation or design of the system.
Goal-C(comply)	To demonstrate compliance of the system with an explicit criterion.

Table 4 The 2-DOF SA vehicle suspension system parameters

m_1	Unsprung mass	36 kg
m_2	Sprung mass	240 kg
c_2	Suspension damping coefficient	1400 Ns/m
k_1	Tire stiffness coefficient	160,000 N/m
k_2	Suspension stiffness coefficient	16,000 N/m
g	Gravity acceleration	9.81 m/s^2
Ω_0	Reference spatial frequency	0.1 m^{-1}
$S_g(\Omega_0)$	Degree of roughness	128×10^{-6} m^2/cycles/m
v_0	Vehicle speed	72 km/h
w_1	Body acceleration weight factor	0.9
w_2	Suspension deformation weight factor	0.05
w_3	Tire load weight factor	0.05

Table 5 Micro-GA parameters

External cycle	100
Internal cycle	4
External population	50
Internal population	6
Replaceable population	2
Crossover probability	0.9
a_0 initial range	[−100, 100]
a_1 initial range	[−100, 100]
a_2 initial range	[−100, 100]

Table 6 A set of polynomial function coefficients for a_i by MOμGA

$\{a_2, a_1, a_0\}\|_{K_e}$	a_i coefficients of K_e	{−3.3, 2.11, 0.31}
$\{a_2, a_1, a_0\}\|_{K_{ec}}$	a_i coefficients of K_{ec}	{0.08, −0.19, −10.12}
$\{a_2, a_1, a_0\}\|_{K_u}$	a_i coefficients of K_u	{5.34, 0.61, 15.42}
$\{a_2, a_1, a_0\}\|_{\alpha}$	a_i coefficients of α	{−0.09, −0.22, 0.92}
$\{a_2, a_1, a_0\}\|_{c_0}$	a_i coefficients of c_0	{0.04, 1.56, 4999.04}
$\{a_2, a_1, a_0\}\|_{\delta}$	a_i coefficients of δ	{4.34, 1.86, 25.15}
$\{a_2, a_1, a_0\}\|_{\lambda}$	a_i coefficients of λ	{0.46, 0.26, 9.64}

PSFαSMC in Table 4. The numerical results are obtained using a specially devised simulation toolkit of micro-GA for MATLAB, known henceforth here as SGALAB [71]. Unless stated otherwise, all the results are generated using the parameters of the genetic algorithms as listed in Table 5, in which binary encoding/decoding, tournament selection, single point crossover, and mutation are utilized by the micro-GA evolutionary process, and a set of polynomial function coefficients a_i by micro-GA is given in Table 6.

As discussed in Sec. 6.1, there are three performance indexes for the vehicle suspension system, which includes body acceleration y_1, tire deformation y_2, and suspension deformation y_3. In this context, the results for the three indexes are applied to

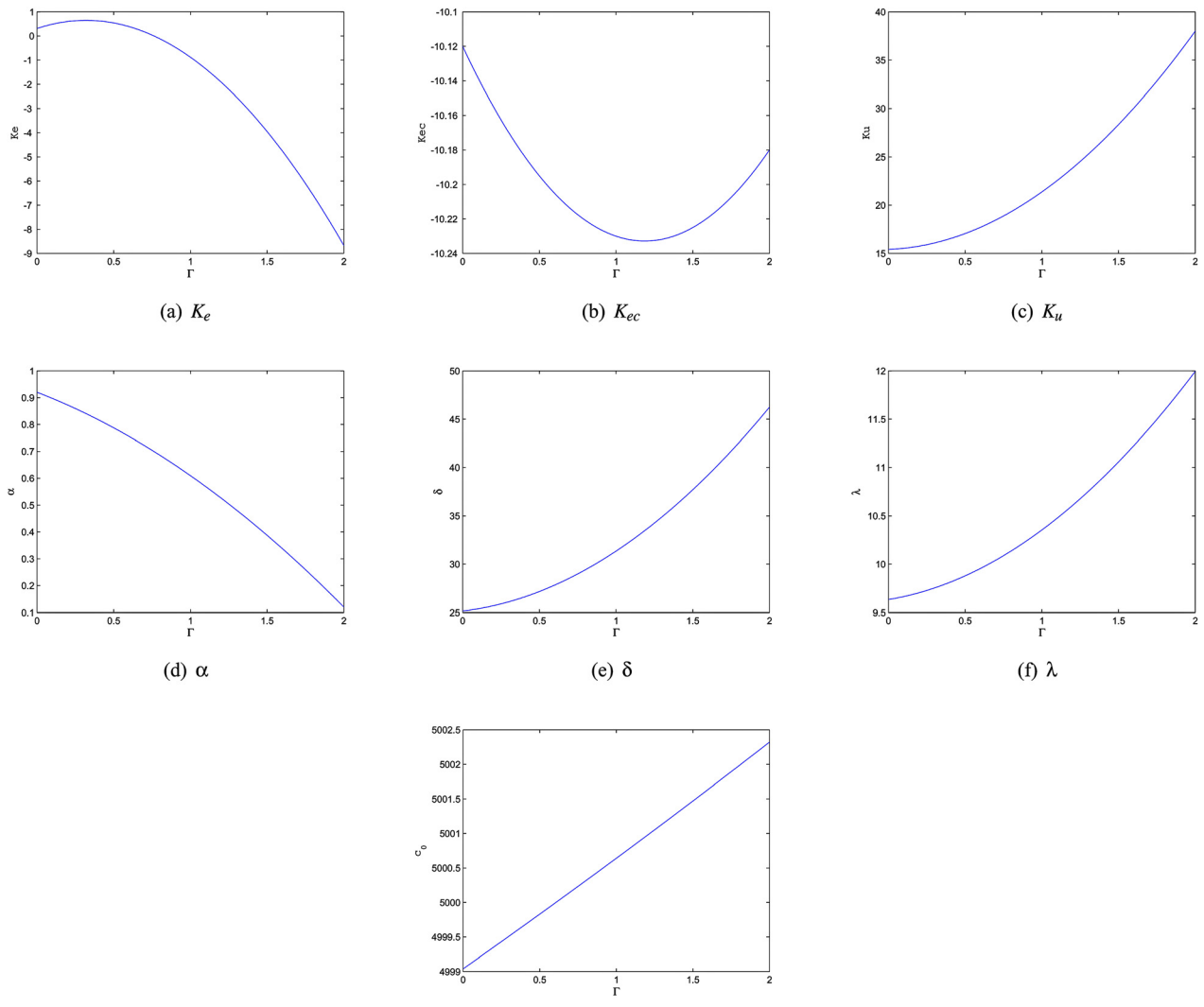

(a) K_e (b) K_{ec} (c) K_u

(d) α (e) δ (f) λ

(g) c_0

Fig. 14 Polynomial supervising functions of PSFαSMC parameters for ride comfort control

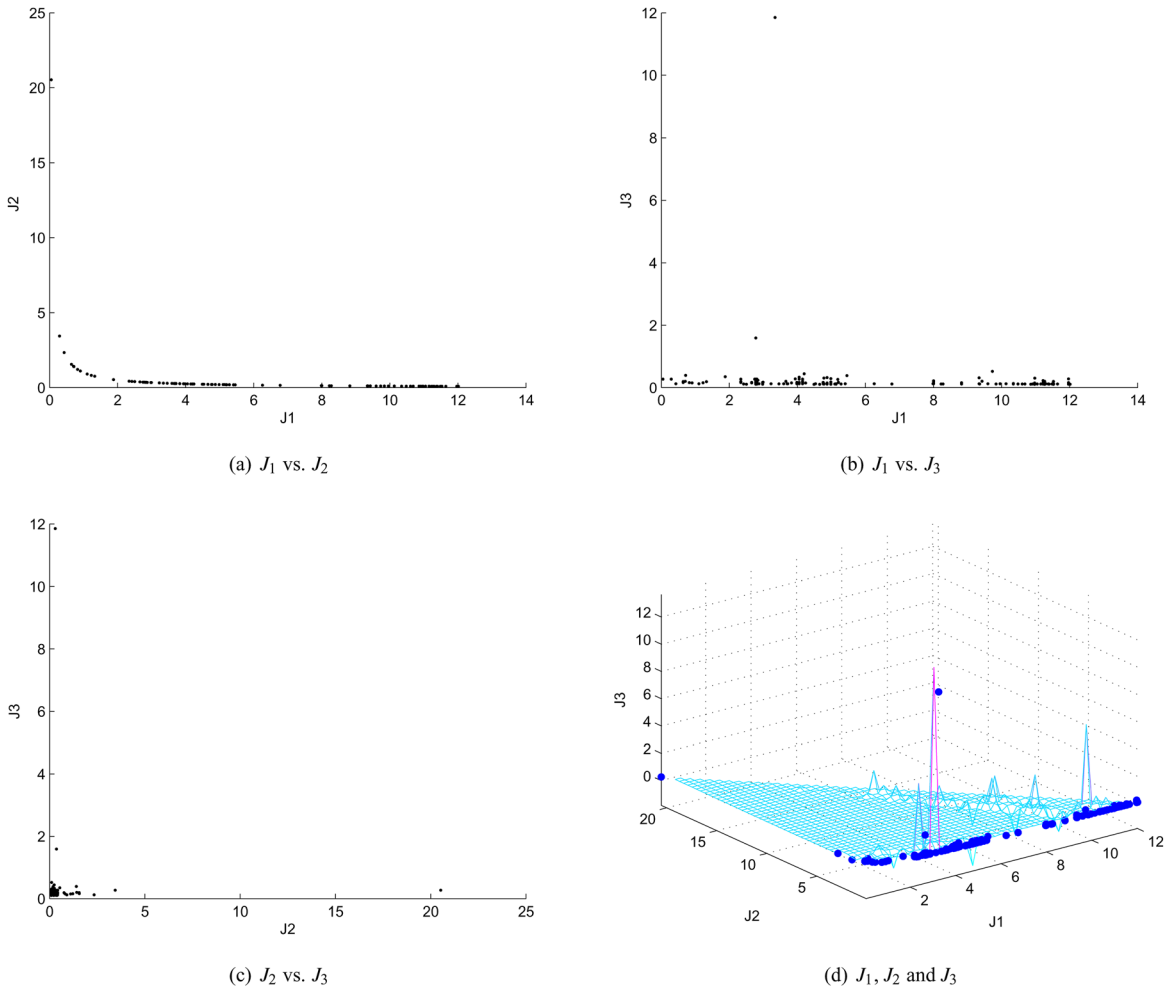

(a) J_1 vs. J_2

(b) J_1 vs. J_3

(c) J_2 vs. J_3

(d) J_1, J_2 and J_3

Fig. 15 Fitness functions—J_1, J_2, and J_3

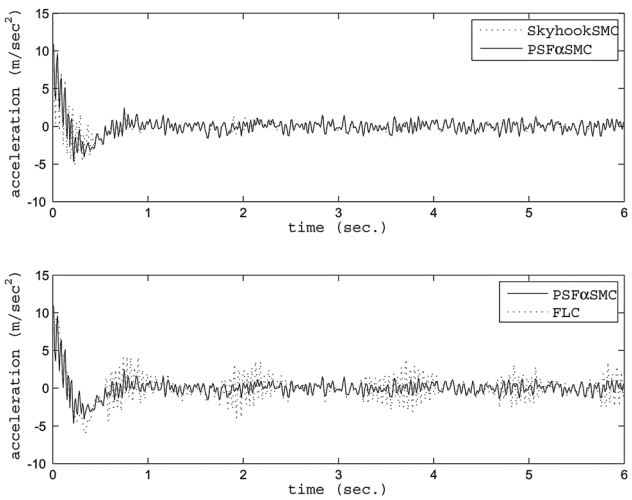

Fig. 16 Vehicle body acceleration y_1 response in time domain

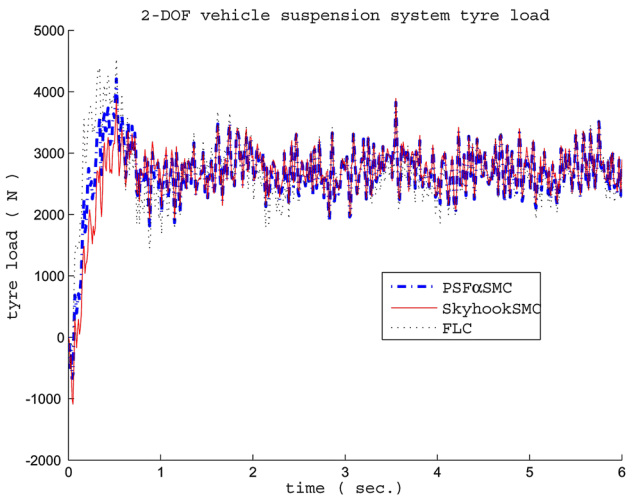

Fig. 17 Tyre load response y_2 in time domain

evaluate the performance for the ride comfort of the 2-DOF SA vehicle suspension system.

The PSFαSMC parameters require a judicious choice as follows: (1) the FLC scaling gains of K_e and K_{ec} for fuzzification of e and ec, respectively, K_u is the defuzzification gain factor; (2) the SkyhookSMC damping coefficient c_0, as stated in Eq. (19), is required to expand the normalized controller output force into a practical range. The thickness of the sliding mode boundary layer is given by δ, and the slope of the sliding surface λ, both of δ and λ data come from design step by micro-GA in the offline step; (3) in the PSFαSMC, α is required to balance the control weight between the FLC and SkyhookSMC. It is easy to switch the controller between the SkyhookSMC and FLC with a proper value of α; (4) the coefficients $\{a_2, a_1, a_0\}$ for the polynomial supervising

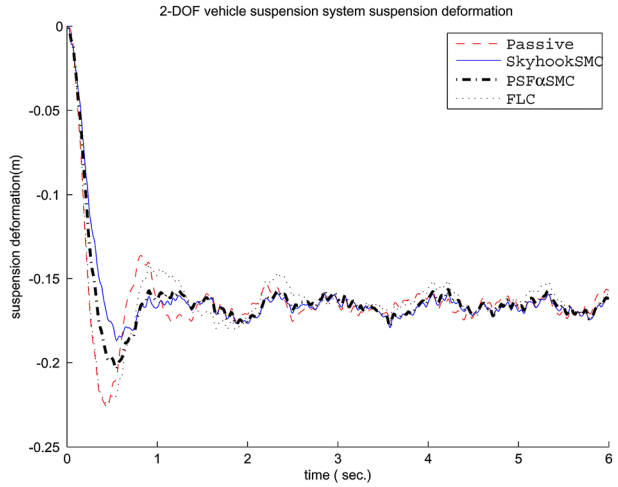

Fig. 18 Suspension deformation y_3 response in time domain

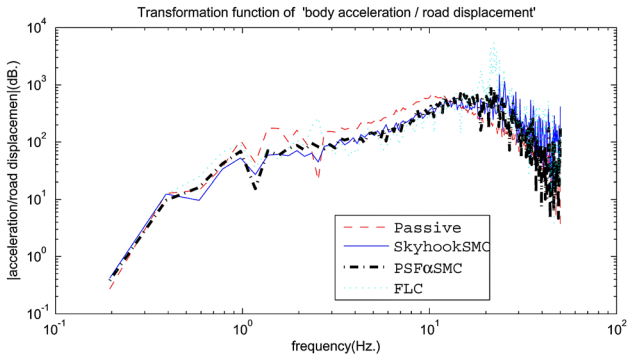

Fig. 19 Vehicle body acceleration response in frequency domain

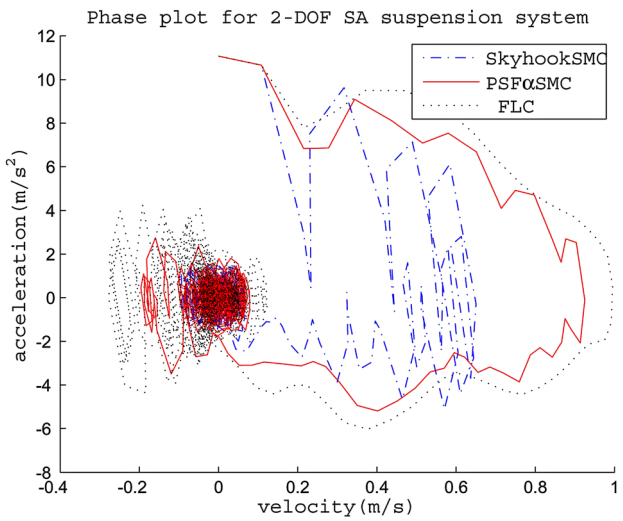

Fig. 20 Vehicle body response phase plot

functions are given in Table 5, which are fitted by the least mean squares algorithm based on data from offline step by micro-GA optimization.

The polynomial functions for K_e, K_{ec}, K_u, α, δ, λ, and c_0 are shown in Figs. 14(*a*)–14(*g*) with a set of coefficients $\{a_2, a_1, a_0\}$, which are listed in Table 6. The coefficients $\{a_2, a_1, a_0\}$ for the polynomial functions are optimized by the micro-GA in offline step, and then applied to the supervising functions for the ride

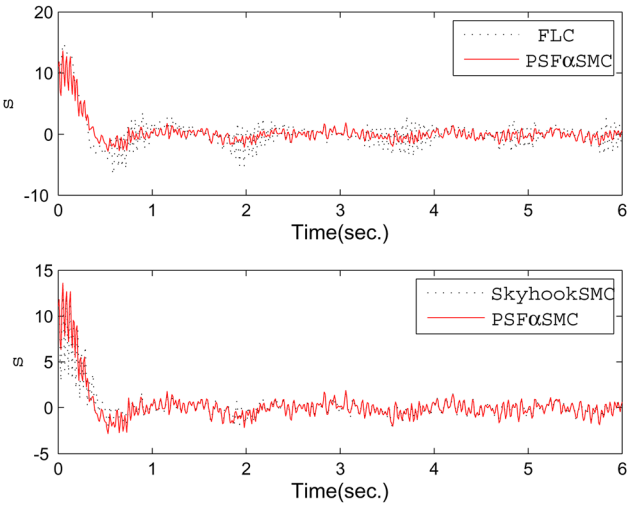

Fig. 21 Sliding surface switching plot

Table 7 Parameters for uncertainty analysis—PSFαSMC ($\alpha = 0.5$, FαSMC)

Statistics	y_1	y_2	y_3	s
Max	11.06	4210.26	0.00	13.58
Min	−4.64	−671.54	−0.20	−2.79
Mean	0.0093	2669.26	−0.16	0.24
Median	0.0074	2699.63	−0.16	−0.061
Mode	−4.64	−671.54	−0.20	−2.79
STD	1.31	531.63	0.026	2.055
Variance	1.72	282632.53	0.00071	4.22
Skewness	3.20	−2.52	4.33	3.88
Kurtosis	27.60	15.35	23.99	20.58

comfort control in online step. As can be seen from Figs. 14(*a*) to 14(*g*), the coefficients $\{a_2, a_1, a_0\}$ can take direct effects on the shapes of the polynomial functions.

With the initial conditions for the micro-GA listed in Table 5, the evolutionary process for each fitness function is listed in Fig. 15, in which Figs. 15(*a*), 15(*b*), and 15(*c*) are the Pareto datasets for, respectively, J_1 versus J_2, J_1 versus J_3, and J_2 versus J_3, and Fig. 15(*d*) is a 3-D surface for the relationship among J_1, J_2, and J_3, in which the position with higher scatter data density means the Pareto optimal of "trade-off" solutions; a set of polynomial function coefficients a_i for one of the selected Pareto front is given in Table 6.

Figure 16 gives the suspension vertical behavior of the body accelerations, PSFαSMC has a better control effect than the FLC and SkyhookSMC on the vehicle body acceleration, and both the PSFαSMC and SkyhookSMC methods can provide better ride comfort control effects than those of the FLC method on the 2-DOF SA suspension system.

Figure 17 shows the tire load response, PSFαSMC and SkyhookSMC methods have the similar tire load level, which is smaller (better) than that of FLC method for the 2-DOF SA suspension system. As shown in Fig. 17, the tire load responses start from 0 N at 0 s, then up to about 4000 N at about 0.5 s and about 3000 N at 1.0 s, in which the 0–1.0 s duration is the transient phase with the gravity's effect on the initially loose (uncompressed) SA suspension; then the timing starts from about at 1 s, the tire load responses step into the steady phase to the simulation end. The transient phase (0 to about 1.0 s) and the steady phase (1.0 s to simulation end) demonstrate the tire load responses' dynamical behaviors under the initial gravity impact and the road roughness, respectively, which validate the control effects for the SA suspension system with discrete and continuous disturbances.

Table 8 Parameters for uncertainty analysis—PSFαSMC (α = 1.0, FLC)

Statistics	y_1	y_2	y_3	s
Max	11.06	4534.98	0.00	14.81
Min	−6.032	−513.78	−0.22	−6.55
Mean	0.0027	2659.48	−0.16	0.23
Median	−0.076	2640.38	−0.16	0.11
Mode	−6.032	−513.78	−0.22	−6.55
STD	1.93	560.63	0.028	2.77
Variance	3.74	314312.74	0.00079	7.71
Skewness	1.25	−0.73	3.10	2.66
Kurtosis	9.53	8.98	18.93	13.79

Table 9 Parameters for uncertainty analysis—PSFαSMC (α = 0.0, SkyhookSMC)

Statistics	y_1	y_2	y_3	s
Max	11.06	3890.82	0	12.99
Min	−5.11	−1089.93	−0.18	−2.15
Mean	0.010	2647.74	−0.16	0.24
Median	−0.0045	2714.45	−0.16	−0.031
Mode	−5.11	−1089.93	−0.18	−2.15
STD	1.26	577.50	0.027	1.83
Variance	1.61	333507.072	0.00073	3.37
Skewness	3.39	−3.07	4.49	4.17
Kurtosis	31.05	16.65	23.55	23.84

Figure 18 shows the relative displacement (suspension deformation) between vehicle sprung mass and unsprung mass. Compared with passive suspension deformation, PSFαSMC, SkyhookSMC, and FLC methods can reduce the 2-DOF SA suspension deformation, and the PSFαSMC and SkyhookSMC methods have a similar suspension deformation level, all of whose suspension deformation is smaller than that of the FLC and passive suspension system. That is, PSFαSMC can provide better ride comfort performance for the 2-DOF SA suspension system.

Figure 19 is the body acceleration in frequency domain, which shows that the control methods of PSFαSMC, SkyhookSMC, and FLC can reduce the amplitudes at two of the key resonance points (10^0 Hz and 10^1 Hz). It also shows that the PSFαSMC can have better control effects on the 2-DOF SA suspension system ride comfort than the FLC and the SkyhookSMC methods for the 2-DOF SA suspension system, and in higher frequency range (>10 Hz) PSFαSMC has better performance than the other controllers, to some extent.

The phase plot (body velocity versus body acceleration) is shown in Fig. 20 as the limit cycles, which represented the improved ride comfort performance of the 2-DOF SA suspension body vertical vibration with controllers. The curves, which corroborated the 2-DOF SA suspension system's interpretations of steady-state, started from the initial value point of (0, g) and gathered to the stable area around (0, 0) in close-wise direction. The PSFαSMC goes faster than FLC, and smoother than SkyhookSMC to the steady-state area.

Figure 21 shows that all the 2-DOF SA suspension system's sliding surfaces are switching and going around $s = 0$, and the PSFαSMC has the smaller and smoother switching behavior than that of the FLC and the SkyhookSMC for the ride comfort control.

The characteristics of the vehicle suspension system's uncertainty measures are given in Tables 7–9, in which the measures of the maximal (Max), the minimal (Min), the central (Mean, Median, and Mode), the dispersion (STD, Variance), asymmetry (Skewness), and flatness (Kurtosis) [69,70,72] can be obtained by estimating the corresponding values of the variable of interest Y and s, and the uncertainty measures have been matched to the figures for the system outputs as discussed above.

10 Conclusions and Future Work

In conclusion, the architecture of the proposed PSFαSMC method has been discussed in which the MOμGA is utilized to optimize the parameters for the polynomial functions in the offline step, and then the polynomial functions are applied to supervise the parameter generation in the online step for the SA suspension ride comfort control. The simulation results demonstrate that the PSFαSMC can adjust control effects between the FLC and the SkyhookSMC by the factor α, which provides flexible control effects for the ride comfort under road uncertainty. Generally, the framework of the PSFαSMC, which can provide a multistate ($\alpha = 0$, 0.5, and 1) control effects, has been approved by the simulation results; some other control methods such as H_∞ and proportional-integral-derivative (PID) control can also be one of the control states. In this paper, the controlled state responses' comparison of FLC, SkyhookSMC, and PSFαSMC validates the effectiveness of the last control method with uncertainty analysis. In the offline step, the MOμGA is applied as an optimizer for the parameters of the polynomial functions, and the optimized results conform to the usability of the MOμGA as a practical approach. In the online step, the optimized polynomial functions are supervising the control effects for the ride comfort and provide an efficient way to adjust the key parameters of the PSFαSMC controller.

With the flexibility of the parameter selection, the PSFαSMC method can be applied to a wide range of engineering applications, such as space tether deployment and vehicle navigation system; according to the requirements of each type of engineering application, some other new methods can also be modulized as the derivatives under the design framework of this proposed PSFαSMC, for example, a central pattern generator for the locomotion control of a legged robot or a propelled robotic fish optimized by the swarm intelligence methods.

Acknowledgment

The authors would like to acknowledge the partial supports provided by the National Natural Science Foundation of China (NSFC) Nos. 51105061 and 30872183. Also, the authors would like to acknowledge the anonymous reviewers with their valuable comments for this paper.

Nomenclature

m_1; m_2 = unsprung mass; sprung mass
k_1; k_2 = tire stiffness coefficient; suspension stiffness coefficient
c_2; c_e = suspension damping coefficient; semi-active suspension damping coefficient
z_1; z_2 = displacement of unsprung mass; displacement for sprung mass
q = road disturbance
v_0 = vehicle speed
g = acceleration of gravity
f_d = semi-active control force
f_{tire} = tire load
$X; Y; U; Q$ = state matrix; output matrix; input matrix; road disturbance matrix
$A; B; C; D; E; F$ = coefficient matrices
y_1 = body acceleration
y_2 = tire deformation
y_3 = suspension deformation
$y_1|_{\text{ref}}$ = the reference state variable for y_1
$y_2|_{\text{ref}}$ = the reference state variable for y_2
$y_3|_{\text{ref}}$ = the reference state variable for y_3
x_1 = tire deformation
x_2 = suspension deformation
x_3 = unsprung mass velocity
x_4 = sprung mass velocity
α = switching factor
s = sliding surface

V = Lyapunov function
c_0 = positive damping ratio for SkyhookSMC
e = error
ec = change-in-error
$H(*)$ = the error state function
E = fuzzified error
EC = fuzzified change-in-error
$u_{F\alpha SMC}$ = control force by the FαSMC
u_{FLC} = control force by the FLC
$u_{SkyhookSMC}$ = control force by the SkyhookSMC
K_e; K_{ec}; K_u = gain factor for e; gain factor for ec; gain factor for u
δ = thickness of the sliding mode boundary layer
λ = slope of the sliding surface
J_1; J_2; J_3 = fitness function for y_1; fitness function for y_2; fitness function for y_3
a_i = constants for the polynomial functions
$\Gamma(*)$ = weighted index
Ω; Ω_0; $S_g(\Omega_0)$ = spatial frequency; reference spatial frequency; degree of roughness
w_1; w_2; w_3 = body acceleration weight factor; tire load weight factor; suspension deformation weight factor
RMS = root mean square
ITAE = the integral of time times the absolute error

References

[1] Yi, K., Wargelin, M., and Hedrick, K., 1993, "Dynamic Tire Force Control by Semi-Active Suspensions," ASME J. Dyn. Syst., Meas., Control, **115**(3), pp. 465–474.
[2] Karnopp, D. C., Crosby, M. J., and Harwood, R. A., 1974, "Vibration Control Using Semi-Active Force Generators," ASME J. Eng. Ind., **94**, pp. 619–626.
[3] Jalili, N., 2002, "A Comparative Study and Analysis of Semi-Active Vibration-Control Systems," ASME J. Vibr. Acoust., **124**(4), pp. 593–605.
[4] Stanway, R., 1996, "The Development of Force Actuators using ER and MR Fluid Technology," *IEE Colloquium on Actuator Technology: Current Practice and New Developments* (*Digest No: 1996/110*), pp. 6/1–6/5.
[5] Spencer, B. F., Jr., Dyke, S. J., Sain, M. K., and Carlson, J. D., 1997, "Phenomenological Model of Magnetorheological Damper," J. Eng. Mech., **123**(3), pp. 230–238.
[6] Caracoglia, L., and Jones, N., 2007, "Passive Hybrid Technique for the Vibration Mitigation of Systems of Interconnected Stays," J. Sound Vib., **307**(3–5), pp. 849–864.
[7] Zhou, Q., Nielsen, S., and Qu, W., 2008, "Semi-Active Control of Shallow Cables With Magnetorheological Dampers Under Harmonic Axial Support Motion," J. Sound Vib., **311**(3–5), pp. 683–706.
[8] Emelyanov, S. V., 1967, *Variable Structure Control Systems*, Nauka, Moscow (in Russian).
[9] Itkis, Y., 1976, *Control Systems of Variable Structure*, Wiley, New York.
[10] Utkin, V. A., 1978, *Sliding Modes and Their Application in Variable Structure Systems*, Nauka, Moscow (in Russian) (also Mir, Moscow, 1978, in English).
[11] Slotine, J.-J. E., and Li, W.-P., 1991, *Applied Nonliear Control*, Prentice-Hall, Englewood Cliffs, NJ.
[12] Hung, J. Y., Gao, W., and Hung, J. C., 1993, "Variable Structure Control: A Survey," IEEE Trans. Ind. Electron., **40**(1), pp. 2–22.
[13] Zadeh, L. A., 1965, "Fuzzy Sets," Inf. Control, **8**(3), pp. 338–353.
[14] Ishigame, A., Furukawa, T., Kawamoto, S., and Taniguchi, T., 1991, "Sliding Mode Controller Design Based on Fuzzy Inference for Non-Linear System," *International Conference on Industrial Electronics, Control and Instrumentation*, Kobe, Japan, Oct. 28–Nov. 1, Vol. 3, pp. 2096–2101.
[15] Ishigame, A., Furukawa, T., Kawamoto, S., and Taniguchi, T., 1993, "Sliding Mode Controller Design Based on Fuzzy Inference for Nonlinear Systems," IEEE Trans. Ind. Electron., **40**(1), pp. 64–70.
[16] O'Dell, B., 1997, "Fuzzy Sliding Mode Control: A Critical Review," Advanced Control Laboratory, Oklahoma State University, Technical Report ACL-97-001.
[17] Ng, K. C., Li, Y., Murray-Smith, D. J., and Sharman, K. C., 1995, "Genetic Algorithm Applied to Fuzzy Sliding Mode Controller Design," *First International Conference on Genetic Algorithms in Engineering Systems: Innovations and Applications, GALESIA*, Sep. 12–14, pp. 220–225.
[18] Kung, C., and Kao, W., 1998, "GA-Based Grey Fuzzy Dynamic Sliding Mode Controller Design," *The 1998 IEEE International Conference on Fuzzy Systems Proceedings, IEEE World Congress on Computational Intelligence*, Anchorage, AK, Vol. 1, pp. 583–588.
[19] Chen, P. C., Chen, C. W., and Chiang, W. L., 2009, "GA-Based Fuzzy Sliding Mode Controller for Nonlinear Systems," Expert Sys. Applic., **36**(3), pp. 5872–5879.
[20] Lo, J. C., and Kuo, Y. H., 1998, "Decoupled Fuzzy Sliding-Mode Control," IEEE Trans. Fuzzy Syst., **6**, pp. 426–435.
[21] Choi, B. J., Kwak, S. W., and Kim, B. K., 1999, "Design of a Single-Input Fuzzy Logic Controller and Its Properties," Fuzzy Sets Syst., **106**, pp. 299–308.
[22] Kung, C., Chen, T., and Kung, L., 2005, "Modified Adaptive Fuzzy Sliding Mode Controller for Uncertain Nonlinear Systems," IEICE Trans. Fundamentals, **E88-A**(5), pp. 1328–1334.
[23] Wang, J., Rad, A. B., and Chan, P. T., 2001, "Indirect Adaptive Fuzzy Sliding Mode Control: Part I: Fuzzy Switching," Fuzzy Sets Syst., **122**(1), pp. 21–30.
[24] Wang, C. H., Liu, H. L., and Lin, T. C., 2002, "Direct Adaptive Fuzzy-Neural Control With State Observer and Supervisory Controller for Unknown Nonlinear Dynamical Systems," IEEE Trans. Fuzzy Syst., **10**, pp. 39–49.
[25] Yau, H. T., and Chen, C. L., 2006, "Chattering-Free Fuzzy Sliding-Mode Control Strategy for Uncertain Chaotic Systems," Chaos, Solitons Fractals, **30**, pp. 709–718.
[26] Eksin, I., Güzelkaya, M., and Tokat, S., 2002, "Self-Tuning Mechanism for Sliding Surface Slope Adjustment in Fuzzy Sliding Mode Controllers," Proc. Inst. Mech. Eng., Part I: J. Syst. Control Eng., **216**(5), pp. 393–406.
[27] Iglesias, E., García, Y., Sanjuan, M., Camacho, O., and Smith, C., 2007, "Fuzzy Surface-Based Sliding Mode Control," ISA Trans., **46**(1), pp. 73–83.
[28] Roopaeia, M., Zolghadrib, M., and Meshksarc, S., 2009, "Enhanced Adaptive Fuzzy Sliding Mode Control for Uncertain Nonlinear Systems," Commun. Nonlinear Sci. Numer. Simul., **14**(9–10), pp. 3670–3681.
[29] Holland, J., 1975, *Adaptation in Natural and Artificial Systems*, University of Michigan Press, Ann Arbor, MI.
[30] Chen, Y., and Zhang, G.-F., 2012, "Exchange Rates Determination Based on Genetic Algorithms Using Mendel's Principles: Investigation and Estimation Under Uncertainty," Inf. Fusion, http://dx.doi.org/10.1016/j.inffus.2011.12.003
[31] Chen, Y., and Song, Z.-J., 2012, "Spatial Analysis for Functional Region of Suburban-Rural Area Using Micro Genetic Algorithm With Variable Population Size," Expert Sys. Applic., **39**(7), pp. 6469–6475.
[32] Chen, Y., Ma, Y., Lu, Z., Peng, B., and Chen, Q., 2011, "Quantitative Analysis of Terahertz Spectra for Illicit Drugs Using Adaptive-Range Micro-Genetic Algorithm," J. Appl. Phys., **110**(4), p. 044902.
[33] Chen, Y., Ma, Y., Lu, Z., Qiu, L.-X., and He, J., 2011, "Terahertz Spectroscopic Uncertainty Analysis for Explosive Mixture Components Determination Using Multi-Objective Micro Genetic Algorithm," Adv. Eng. Software, **42**(9), pp. 649–659.
[34] Chen, Y., Ma, Y., Lu, Z., Xia, Z.-N., and Cheng, H., 2011, "Chemical Components Determination via Terahertz Spectroscopic Statistical Analysis Using Micro Genetic Algorithm," Opt. Eng., **50**(3), p. 034401.
[35] Chen, Y., and Cartmell, M. P., 2007, "Multi-Objective Optimisation on Motorized Momentum Exchange Tether for Payload Orbital Transfer," 2007 IEEE Congress on Evolutionary Computation (CEC), Singapore, Sept. 25–28.
[36] Krishnakumar, K., 1989, "Micro-Genetic Algorithms for Stationary and Non-Stationary Function Optimization," Proc. SPIE, **1196**, pp. 289–296.
[37] Goldberg, D., 1989, "Sizing Populations for Serial and Parallel Genetic Algorithms," *Proceedings of the Third International Conference on Genetic Algorithms*, San Mateo, CA, Vol. 1196, pp. 70–79.
[38] Ogata, K., 1996, *Modern Control Engineering*, Prentice-Hall, Englewood Cliffs, NJ.
[39] Chen, Y., 2009, "Skyhook Surface Sliding Mode Control on Semi-Active Vehicle Suspension Systems for Ride Comfort Enhancement," Engineering, **1**(1), pp. 23–32.
[40] Chen, Y., and Cartmell, M. P., 2009, "Hybrid Fuzzy and Sliding-Mode Control for Motorised Tether Spin-Up When Coupled With Axial Vibration," 7th International Conference on Modern Practice in Stress and Vibration Analysis, Sept. 8–10, New Hall, Cambridge, UK.
[41] Chen, Y., and Cartmell, M. P., 2009, "Hybrid Fuzzy Skyhook Surface Sliding Mode Control for Motorised Space Tether Spin-Up Coupled With Axial Oscillation," Advanced Problems in Mechanics, June 30–July 5, Russian Academy of Sciences, St. Petersburg, Russia.
[42] Chen, Y., and Cartmell, M. P., 2010, "Hybrid Sliding Mode Control for Motorised Space Tether Spin-Up When Coupled With Axial and Torsional Oscillation," Astrophys. Space Sci., **326**(1), pp. 105–118.
[43] Chen, Y., 2010, *Dynamical Modelling of Space Tether: Flexible Motorised Momentum Exchange Tether and Hybrid Fuzzy Sliding Mode Control for Spin-Up*, LAP Lambert Academic Publishing AG & Co., Saarbrucken, Germany.
[44] Slotine, J. J. E., 1982, "Tracking Control of Non-Linear Systems Using Sliding Surfaces With Application to Robot Manipulations," Ph.D. dissertation, Laboratory for Information and Decision Systems, Massachusetts Institute of Technology, Cambridge, MA.
[45] Burns, R., 2001, *Advanced Control Engineering*, Butterworth-Heinemann, Oxford.
[46] Passino, K. M., and Yurkovich, S., 1998, *Fuzzy Control*, Addison Wesley Longman, Menlo Park, CA.
[47] Mamdani, E. H., and Assilian, S., 1975, "An Experiment in Linguistic Synthesis With a Fuzzy Logic Controller," Int. J. Man-Mach. Stud., **7**(1), pp. 1–13.
[48] Mamdani, E. H., 1976, "Advances in the Linguistic Synthesis of Fuzzy Controllers," Int. J. Man-Mach. Stud., **8**(1), pp. 669–678.
[49] Mamdani, E. H., 1977, "Applications of Fuzzy Logic to Approximate Reasoning Using Linguistic Synthesis," IEEE Trans. Comput., **26**(12), pp. 1182–1191.
[50] Zadeh, L. A., 1973, "Outline of a New Approach to the Analysis of Complex Systems and Decision Processes," IEEE Trans. Syst. Man Cybern., **3**(1), pp. 28–44.
[51] Chen, Y., Fang, Z., Luo, H., and Deng, Z., 2004, "Simulation Research on Real-Time Polynomial Function Supervising PID Control Based on Genetic Algorithms," J. Syst. Simul., **16**(6), pp. 1171–1174. Available at: http://www.cnki.com.cn/Article/CJFDTotal-XTFZ200406016.htm
[52] Coello Coello, C. A., and Pulido, G., 2001, "A Micro-Genetic Algorithm for Multiobjective Optimization," *Proceedings of the Genetic and Evolutionary Computation Conference*, Springer-Verlag, pp. 126–140.

[53] Lo, K. L., and Khan, L., 2004, "Hierarchical Micro-Genetic Algorithm Paradigm for Automatic Optimal Weight Selection in H_∞ Loop-Shaping Robust Flexible AC Transmission System Damping Control Design," IEE Proc.: Gener. Transm. Distrib., **151**(1), pp. 109–118.
[54] Tam, V., Cheng, K. Y., and Lui, K. S., 2006, "Using Micro-Genetic Algorithms to Improve Localization in Wireless Sensor Networks," J. Commun., **1**(4), pp. 1–10.
[55] Davidyuk, O., Selek, I., Ceberio, J., and Riekki, J., 2007, "Application of Micro-Genetic Algorithm for Task Based Computing," *Proceeding of International Conference on Intelligent Pervasive Computing (IPC-07)*, Jeju Island, Korea, October, pp. 140–145.
[56] Szőllős, A., Šmíd, M., and Hájek, J., 2009, "Aerodynamic Optimization via Multi-Objective Micro-Genetic Algorithm With Range Adaptation, Knowledge-Based Reinitialization, Crowding and ε-Dominance," Adv. Eng. Software, **40**(6), pp. 419–430.
[57] Deb, K., and Goldberg, D. E., 1989, "An Investigation of Niche and Species Formation in Genetic Function Optimization," *Proceedings of the Third International Conference on Genetic Algorithms*, J. D. Schaffer, ed., Morgan Kauffman, San Mateo, CA, pp. 42–50.
[58] Goldberg, D., 1989, *Genetic Algorithms in Search, Optimization and Machine Learning*, Kluwer Academic Publishers, Boston, MA.
[59] Fonseca, C. M., and Fleming, P. J., 1993, "Genetic Algorithms for Multiobjective Optimization: Formulation, Discussion and Generalization," *Proceedings of the Fifth International Conference on Genetic Algorithms*, S. Forrest, ed., Morgan Kauffman, San Mateo, CA, pp. 416–423.
[60] International Organization for Standardization, 1997, "Mechanical Vibration and Shock—Evaluation of Human Exposure to Whole-Body Vibration—Part 1: General Requirements," ISO 2631-1:1997.
[61] Sayers, M. W., 1996, "Interpretation of Road Roughness Profile Data," Final Report, Report No. UMTRI-96-19.
[62] Wei, L., Fwa, T. F., Asce, M., and Zhe, Z., 2005, "Wavelet Analysis and Interpretation of Road Roughness," J. Transp. Eng., **131**(2), pp. 120–130.
[63] International Organization for Standardization, 1995, "Mechanical Vibration—Road Surface Profiles—Reporting of Measured Data," ISO 8608:1995.
[64] Wong, J. Y., 2001, *Theory of Ground Vehicles*, 3rd ed., Wiley, New York.
[65] International Organization for Standardization, 1982, "Reporting Vehicle Road Surface Irregularities," ISO/TC108/SC2/WG4 N57.
[66] Elbeheiry, E. M., and Karnopp, D. C., 1996, "Optimal Control of Vehicle Random Vibration With Constrained Suspension Deflection," J. Sound Vib., **189**(5), pp. 547–564.
[67] Ramji, K., Gupta, A., Saran, V. H., Goel, V. K., and Kumar, V., 2004, "Road Roughness Measurements Using PSD Approach," J. Inst. Eng., 85, pp. 193–201.
[68] Liu, Y., Matsuhisa, H., and Utsuno, H., 2008, "Semi-Active Vibration Isolation System With Variable Stiffness and Damping Control," J. Sound Vib., **313**(1–2), pp. 16–28.
[69] Rocquigny, E., Devictor, N., and Tarantola, S., 2008, *Uncertainty in Industrial Practice*, Wiley, New York.
[70] International Organisation for Standardisation, 2008, "The Guide to the Expression of Uncertainty in Measurement (GUM)," ISO/IEC Guide 98-3:2008.
[71] Chen, Y., 2009, "Simple Genetic Algorithm Laboratory Toolbox for MATLAB," http://www.mathworks.co.uk/matlabcentral/fileexchange/5882
[72] Choi, S.-K., Grandhi, R. V., and Canfield, R. A., 2007, *Reliability-Based Structural Design*, Springer-Verlag, London.